Numerical Simulation of Natural Turbulent Convection with Vorticity Vector Formulation

Article *in* IOSR Journal of Mathematics · June 2023

DOI: 10.9790/5728-1903026279

2 authors:

Filentinus Otulo
Kenyatta University
1 PUBLICATION **0** CITATIONS
SEE PROFILE

Awuor Kennedy Otieno
Kenyatta University
22 PUBLICATIONS **22** CITATIONS
SEE PROFILE

IOSR Journal of Mathematics (IOSR-JM)
e-ISSN: 2278-5728, p-ISSN: 2319-765X. Volume 19, Issue 3 Ser. 2 (May. – June. 2023), PP 62-79
www.iosrjournals.org

Numerical Simulation of Natural Turbulent Convection with Vorticity Vector Formulation

Otulo Onyango Filentinus[1], Awuor Kennedy Otieno[2]
School of Pure and Applied Sciences, Kenyatta University, Box 43844 – 00100, Nairobi, Kenya.

Abstract:
Background: *Turbulent natural convection in an enclosure plays a big part in heat transmission and the building environment. Sophisticated buildings around the world are outfitted with costly heaters and coolers to maintain comfortable temperatures for human existence, manufacturing, and sophisticated farming methods, a scenario that many people cannot afford. Over a time, researchers have consistently developed a number of numerical study models to simulate the natural turbulent flow in these rectangular enclosures to solve complex problems associated with turbulent flows. In spite of several experimental studies and model simulations on the structure of natural turbulence convection, the fundamental mechanism in turbulent phenomena is still incomplete. Significant variations in experimental data and model simulation data in previous studies have been noted. This is because the unknown turbulent correlation coefficients resulting from the nonlinear terms of the turbulent flow control equations make it difficult to accurately determine fluid flow variables such as mean velocity distribution, temperature distribution and kinetic energy in a model simulation. Thus, an accurate numerical prediction of natural turbulence convection is crucial to solving the nonlinear equations for subsequent practical applications.*

Methodology: *The performance of a numerical turbulence model k-ε in estimating the amount of heat transfer that occurs as a result of the naturally occurring turbulent convection that takes place within an air-filled rectangular enclosure is investigated in this work using vorticity vector formulation. The workflow of simulating the heat transfer which results from the action of natural convection within an enclosed rectangular cavity takes into account the effect of turbulence for the Rayleigh numbers* $Ra = 1.552 \times 10^{10}$, $Ra = 9.934 \times 10^{11}$, $Ra = 1.552 \times 10^{13}$ *and* $Ra = 2.425 \times 10^{14}$. *The Low-Reynolds-number turbulence. k-ε model was employed in this numerical study to model the non-linear relations* $\overline{\nabla \cdot \rho u' u'}$ *and* $\frac{\partial c_p T' u'}{\partial x_i}$ *in the averaged Navier Stokes equation and energy equation respectively to complete the governing equations. Apart from the hot and cold walls, which are maintained at 308K and 288K, respectively, all of the walls of the enclosure are adiabatic. The vorticity vector formulation allowed the pressure term to be removed from the momentum equation. Finite difference approximations were used in the FLUENT program to solve the vorticity, energy, vector potential, and two resultant equations for each model together with their boundary conditions.*

Results and Conclusion*: The outcomes of the study for the distribution of the velocity and temperature components are presented, demonstrating that the number of contours and vortices increases proportionally with the Rayleigh Number. In addition, a higher Rayleigh number indicates more turbulence, which in turn implies a higher absolute value of the velocity hence increased Kinetic energy.*

Key Words: *Vorticity vector formulation,Vorticity, Stream function, Vector potential, Reynold stress*

Date of Submission: 10-06-2023 Date of Acceptance: 24-06-2023

I. Introduction

The fluid mechanics of today's world are intensely dominated by the chaotic and volatile motion known as turbulent flow. Even if the flow occurs naturally or is forced into the surrounding, heat, momentum, and mass exchange are caused by large-scale irregular vortex movements rather than diffusion. Many thermofluidic devices such as pipes, boilers, compressors, integrated circuit motors, and capacitors are made to withstand the turbulence of the liquid flow around them. The movement of fluids is so closely related to these industrial disciplines of heat and mass transport that it is necessary to calculate turbulent flow before studying these fields.

The process through which heat and mass are transferred in fluids is known as convection, and it is closely related to the computation of heat exchange rates between liquid and solid borders. Laminar and turbulent flows are the two types of convective heat exchange in which the viscosity of the liquid is important. In turbulent flow, small fluid components rotate in the flow direction and perpendicular to it, generating a turbulent mixture, while laminar flow is characterized by fluid elements traveling in parallel but not interacting with each other or the fluid in the adjacent paths.

There are two different kinds of convection, namely natural (free) convection and forced convection. In natural convection, fluid motion is caused solely by density differences derived from temperature gradients i.e., buoyancy driven and not by an external source. With the right surface geometry and orientation, a circular flow cycle of the liquid is created where the fluid around the heat source heats up and undergoes thermal expansion, becoming less dense and rising up while the cooler part of the fluid, which is denser, sinks and displaces the warmer less dense fluid. This cycle only ends when the fluid is evenly heated throughout. If the movement of the fluid is caused by an external force such as stirring, or pumping then we have a forced convection. Also, it's critical to note that the fluid velocity and heat transfer coefficient that occur in natural turbulent flow are generally low compared to forced-controlled or man-controlled turbulent flow. Only natural turbulent convection in rectangular enclosed cavities will be taken into account in this study because it is an active area of research with numerous engineering applications including building insulation, nuclear reactor construction, electronic cooling devices, air conditioning systems, in- door air quality, and solar energy collectors among others. All these applications require a reliable data source for temperature and velocity distribution.

The turbulent convection motion in this project is considered to be buoyancy driven as a result of heating a fraction of one of the vertical walls and cooling an equal fraction of the opposite wall in the enclosure. Hence, maintaining a temperature difference between the two walls that are not adjacent while other walls of the enclosure are considered to be adiabatic.

II. Literature Review

Numerous studies have been performed by different researchers on naturally occurring turbulence convection in enclosed cavities. In a rectangle-shaped confinement with partially insulated walls that trans- port heat at local substructure heating, [1]explored the effects of natural convection on turbulence. This is plausible given how heat is transferred in a frontier environment between convection and radioactivity. The mathematical formalism was based on the conventional k-ε turbulence equations with wall functions. The transient factor, thermal conductivity rate, and the Grashof number were all considered because of their unique impacts.

[2]analyzed naturally occurring convection numerically in a trapezoidal enclosure with a wave-like top surface. In their work they studied the effects of wave amplitude, Rayleigh number and Darcy number on the free convection inside the cavity full of seawater of Prandtl number 7.2 by uniformly heating the bottom and partially heating the inclined boundaries. The results of their study demonstrate that different parameters affect convection motion, and that flow intensities and temperature distributions increase with increasing Rayleigh and Darcy numbers. The results also demonstrate that unlike Rayleigh numbers and Darcy numbers, the wave-like top surface has a negligible impact on the flow field pattern and temperature dispersion. [3]investigated heat transfer and free convective motion in a cylinder by studying the effects of increasing Reynolds, Froude, Euler, and Prandtl numbers on the temperature and velocity. According to the findings of their research, buoyancy forces caused by temperature differences between the top and bottom of cylinders influence significantly the air velocity within the enclosure, and that temperature and velocity are inversely related to cylindrical height.

[4]numerically evaluated models of free convection turbulence in two- and three-dimensional rectangular housing by solving 2D and 3D unsteady state of the governing equations of turbulent using FLUENT 6.3.26. Surface averaged mean Nusselt numbers were used to compare the obtained heat transfer rates for the 2D and 3D RANS models. According to their findings, 3D RANS model produces mean Nusselt numbers that are more accurate than 2D for larger Rayleigh numbers. By creating isotherms and streamlines for various aspect ratios and making an observation on the

impact of the same parameter along hot and cold walls of an enclosure, [5] statistically explored natural convection in rectangular enclosures. According to their study's findings, in horizontal housings heated from the side, the aspect ratio has a substantial influence on the temperature dispersion and fluid flow throughout the housing. It also causes a decrease in speed and leads the vortices to become more parallel, which reduces turbulence.

[6]mathematically analyzed naturally occurring turbulent convection at various aspect ratios and discovered that there is no uniformity to the distribution of velocity and temperature and that the aspect ratio of the enclosed cavity has a substantial impact on both their magnitudes and distributions.

In a large eddy simulation of free turbulent convection in an inclined tall cavity, [7] employed the spectral method to SOLVE the Reyleigh-Benard problem.

[8] conducted a numerical investigation of free turbulent convection inside a rectangular chamber that was heated and cooled in designated zones. Through their studies, they concluded that changing the Rayleigh number affects turbulence via changing the temperature distribution and the flow rate of the fluid.

Through experimental and model studies of heat and mass transfer at Reynolds numbers 40,000 and 80,000, [9]investigated turbulence of internal cooling passages and the search for porous ribs that provide high thermal performance.

Using OpenFOAM, [10]compared the predictions of two turbulence models for low turbulent convection in a rectangular enclosed chamber to the results found in the experimental literature. The results show that near the

isothermal walls, temperature and velocity changed dramatically, and that natural convection caused by turbulence occurred in an air-filled square cavity.

[11]Using a custom Fortran 90 program while utilizing the lattice Boltzmann technique as the foundation, studied the Rayleigh-Bénard Convection numerically. They left the right wall open and added two cozy circular and elliptical feathers to the lower wall. They used the Red- Boltzmann equation, which is connected to the Boussinesq method, to develop the nonlinear associated differential equations. The heat transfer rates from elliptical heat sources were greater than those from circular ones according to the findings of their Code verification, which also demonstrated good dependability of the existing mesoscopic numerical approach.

The foundation of the research by [12]was the variation of cylinder position between eccentric and concentric positions along the enclosure's horizontal and vertical medians and diagonals. They conducted a mathematical study of free convection from a horizontally oriented cylinder at an eccentric position with a variation in aspect ratio of a cooled square cavity. To model the cylinder surface, they used quasi approximation conditions and the submerged boundary method. The heat transfer behavior with respect to Aspect ratio and Rayleigh number was determined using a combo of thermal classificatory effects, enhanced convectional flow, and thermal effect between combustor periphery and enclosure wall. According to their findings, the circumferential location of the cylinder leads to a higher thermal exchange at an Aspect Ratio of 0.15 for Ra of 11140 and Aspect Ratio of 0.175 for Ra of 111400 for idiosyncratic position, and heat transfer was enhanced at the position closest to the vertical at Aspect Ratio greater than 0.175.

Natural turbulent convection modeling in a rectangle-shaped cavity was further carried out by [13] by using a k -ω SST turbulent model while considering the Boussinesq approximations and vector potential approximation to determine the best position of a heater and a cooler in enclosure. Her research's findings demonstrate that turbulence is reduced by rise in Rayleigh number, and that the location of heat source and the cooler has a significant impact on turbulence. As a result, the position of the heater and cooler affects how heat is distributed inside an enclosure. She also recommended placing the cooler and heater on the same side of the wall.

III. Methodology

General Governing Equations

Since the majority of turbulent flows involve mass and heat transfers, it is crucial to take into account the dynamics of energy dissipation, multiple-point correlation, energy spectrum, and scalar transport. This is because explanations of turbulent flows ultimately rest in the physics of the momentum, energy, and vorticity fields as stated [14]In order to set the stage for discussion by creating fundamental equations that will clearly illustrate the physical processes that need to be investigated, understood, or predicted when solving natural turbulent convection, Natural turbulent convection has been studied in this section as a function of fluid flow characteristics in a rectangular enclosure with a fraction of one vertical wall heated and an equivalent percentage of the opposite wall cooled. The partial differential forms of Continuity Equation, Navier Stokes Equation and Energy Equation are presented in cartesian and tensor forms. The stated governing equations are:

$$\frac{\partial \rho}{\partial t} + \frac{\partial}{\partial x_j}(\rho u_j) = 0 \tag{1}$$

$$\rho\left(u\frac{\partial u}{\partial x} + v\frac{\partial u}{\partial y} + w\frac{\partial u}{\partial z} + \frac{\partial u}{\partial t}\right) = -\frac{\partial p}{\partial x} + \mu\left(\frac{\partial^2 u}{\partial x^2} + \frac{\partial^2 u}{\partial y^2} + \frac{\partial^2 u}{\partial z^2}\right) + S_x \tag{2}$$

$$\rho\left(u\frac{\partial v}{\partial x} + v\frac{\partial v}{\partial y} + w\frac{\partial v}{\partial z} + \frac{\partial v}{\partial t}\right) = -\frac{\partial p}{\partial y} + \mu\left(\frac{\partial^2 v}{\partial x^2} + \frac{\partial^2 v}{\partial y^2} + \frac{\partial^2 v}{\partial z^2}\right) + S_y \tag{3}$$

$$\rho g_i - \frac{\partial P}{\partial x_i} + \frac{\partial}{\partial x_j}\left[\mu\left(\frac{\partial u_i}{\partial x_j} + \frac{\partial u_j}{\partial x_i}\right) + \mu_s \delta_{ij}\frac{\partial u_k}{\partial x_k}\right] = \frac{\partial}{\partial t}(\rho u_i) + \frac{\partial}{\partial x_j}(\rho u_i u_j) \tag{4}$$

$$\frac{\partial}{\partial t}\rho C_p T + \frac{\partial}{\partial x_j}(\rho C_p u_j T) = \frac{\partial}{\partial x_j}\left(\lambda\frac{\partial T}{\partial x_j}\right) + \beta T\left(\frac{\partial p}{\partial t} + \frac{\partial u_j p}{\partial x_j}\right) + \tau_{ij}\frac{\partial u_j}{\partial x_j} \tag{5}$$

Final Sets of Equation

On statistically averaging and decomposition of the governing equations by Reynolds Decomposition method, the following final sets of equations were obtained and made simpler by taking the over-bar in the preceding time-averaged equation for mean values of the variables throughout time and replaced by upper case, while the prime denoting the fluctuating quantities are written in lower case. Below are the complete set of equations for turbulent natural convection.

$$\frac{\partial \bar{\rho}}{\partial t} + \frac{\partial}{\partial x_j}\left(\overline{\rho U_j}\right) + \frac{\partial}{\partial x_j}\left(\overline{\rho' U_j'}\right) = 0 \quad (6)$$

$$\frac{\partial}{\partial t}\left(\overline{\rho u_\iota} + \overline{\rho' u_\iota'}\right) + \frac{\partial}{\partial x_j}\left(\overline{\rho u_\iota u_j} + \overline{u_t \rho' u_j}\right) = -\frac{\partial \bar{p}}{\partial x_i} + \bar{\rho} g_i + \frac{\partial}{\partial x_j}\left(\overline{\tau_{\iota j}} - \overline{u_j \rho' u_\iota'} - \overline{\rho u_t' u_j'} - \overline{\rho' u_\iota' u_j'}\right) \quad (7)$$

And $\overline{\tau_{\iota j}} = \mu\left(\frac{\overline{\partial u_\iota}}{\partial x_j} + \frac{\partial \overline{u_j}}{\partial x_i}\right) + \mu_s \delta_{iy} \frac{\partial \pi_k}{\partial x_k}$

where REYNOLDS STRESS EQUATION is given by $\overline{\nabla \cdot \rho u_\iota' u_j'}$

$$\frac{\partial}{\partial t}\left(C_p \overline{\rho T} + C_p \overline{\rho' T'}\right) + \frac{\partial}{\partial x_j}\left(C_p \overline{\rho u_j T}\right) = \frac{\partial \bar{p}}{\partial t} + \frac{\partial \bar{p}}{\partial x_j} + \overline{u_\iota' \frac{\partial p'}{\partial x_j}} + \frac{\partial}{\partial x_j}\left(\lambda \frac{\partial \bar{T}}{\partial x_j} - C_p \overline{\rho u_\iota' T'} - C_P \overline{\rho' u_\iota T'}\right) + \bar{\Phi} \quad (8)$$

Where $\bar{\Phi} = \overline{\tau_{\iota j}} \frac{\partial \overline{u_\iota}}{\partial x_j} + \overline{\tau_{\iota j}' \frac{\partial u_\iota'}{\partial x_j}}$ and $\frac{\partial C_p \overline{T' u_\iota'}}{\partial x_j}$ represent the thermal fluxes

$$\frac{\partial}{\partial t}(\bar{\rho} k) + \frac{\partial}{\partial x_j}\left(\overline{\rho u_j k}\right) = \overline{u_j' \frac{\partial}{\partial x_j} \tau_{\iota j}} - \frac{1}{2}\frac{\partial}{\partial x_j}\left(\overline{\rho u_\iota' u_\iota' u_j'}\right) - \overline{\rho u_\iota' u_j'} \frac{\partial u_i}{\partial x_j} + \overline{\rho' u_\iota' g_\iota} - \overline{u_j' \frac{\partial p'}{\partial x_\iota}} \quad (9)$$

$$\frac{\partial}{\partial t}\bar{\rho}\varepsilon + \frac{\partial}{\partial x_j}\overline{\rho u_j}\varepsilon = -\frac{\partial}{\partial x_k}\left(\overline{\mu \mu_k' \frac{\partial u_\iota'}{\partial x_j}\frac{\partial u_\iota'}{\partial x_j}} + 2v \overline{\frac{\partial u_k'}{\partial x_\iota}\frac{\partial p'}{\partial x_\iota}}\right) - 2\mu \overline{\frac{\partial u_\iota'}{\partial x_k}\frac{\partial u_\iota'}{\partial x_j}\frac{\partial u_j'}{\partial x_j}} - 2\bar{\rho} v \overline{\frac{\partial^2 u_\iota'}{\partial x_k \partial x_j}}^2 + 2v \overline{\frac{\partial u_\iota'}{\partial x_j}\frac{\partial \rho'}{\partial x_j}} g_i$$
$$-2\mu \frac{\partial \bar{u}_i}{\partial x_k}\left(\overline{\frac{\partial u_\iota'}{\partial x_\iota}\frac{\partial u_k'}{\partial x_j}} + \overline{\frac{\partial u_j'}{\partial x_i}\frac{\partial u_j'}{\partial x_k}}\right) - 2\mu \overline{\frac{\partial^2 u_\iota}{\partial x_j \partial x_k} u_k' \frac{\partial u_\iota}{\partial x_j}} \quad (10)$$

Non Dimensionalization

We have adopted suitable dimensionless schemes in this study to reduce the number of parameters that are involved in the description of turbulent flow as well as to make the solutions bounded, for instance temperature can be made dimensionless such that it varies from 0 to 1.

The following equations and dimensionless parameters were obtained upon the non – dimensionalization of the final sets of equations while taking U and T as the dimensionless velocity and temperature components respectively

$$\frac{\partial \rho}{\partial t} + \frac{\partial}{\partial x_j}\left(\rho U_j + \overline{\rho U_j}\right) = 0 \quad (11)$$

$$\frac{\partial}{\partial t}\left(\rho U_i + \overline{\rho u_\iota}\right) + \frac{\partial}{\partial x_i}\left(\rho U_i U_j + U_i \overline{\rho u_j}\right) = -B_1 \frac{\partial p}{\partial x_i} + B_2 \rho g_i \frac{\partial}{\partial x_i}\left(B_3 \tau_{ij} - U_j \overline{\rho u_j} - \overline{\rho u_\iota u_J}\right) \quad (12)$$

$$\frac{\partial}{\partial t}\left(C_p \rho \Theta + C_p \overline{\rho \Theta}\right) + \frac{\partial}{\partial x_j}\left(C_p \rho U_j \Theta\right) = M_1\left[\frac{\partial p}{\partial t} + U_j \frac{\partial p}{\partial x_j} + \overline{u_j \frac{\partial p}{\partial x_J}}\right] + \frac{\partial}{\partial x_j}\left(M_2 \lambda \frac{\partial \Theta}{\partial x_j} - C_p \rho \overline{u_\iota \Theta} - C_p \rho u_i \Theta\right) + M_3 \Phi \quad (13)$$

$$\frac{\partial}{\partial t}\rho k + \frac{\partial}{\partial x_j}\rho U_j k = T_1 \overline{u_j \frac{\partial}{\partial x_j} u_j \left(\frac{\partial u_J}{\partial x_j} + \frac{\partial u_J}{\partial x_j}\right)} - \frac{1}{2}\frac{\partial}{\partial x_j}\rho \overline{u_\iota u_j}\frac{\partial U_i}{\partial x_j} + T_2 \overline{\rho u_\iota g_\iota} - T_3 \overline{u_j}\frac{\partial p}{\partial x_i} \quad (14)$$

$$\frac{\partial}{\partial t}\rho\varepsilon + \frac{\partial}{\partial x_j}\rho U_j \varepsilon = -\frac{\partial}{\partial x_k}\left(A_1 \mu u_k \frac{\partial u_i}{\partial x_j}\frac{\partial u_j}{\partial x_j} + 2A_2 V \overline{\frac{\partial u_k}{\partial x_\iota}\frac{\partial \rho}{\partial x_\iota}} - A_1 \mu \frac{\partial \varepsilon}{\partial x_k}\right) - 2A_1 \mu \frac{\partial U_i}{\partial x_j}\left(\overline{\frac{\partial u_\iota}{\partial x_J}\frac{\partial u_k}{\partial}} + \overline{\frac{\partial u_J}{\partial x_J}\frac{\partial u_J}{\partial x_k}}\right) -$$
$$2A_1 \mu \frac{\partial^2 U_i}{\partial x_j \partial x_k} \overline{\mu \mu u_k \frac{\partial u_\iota}{\partial x_j}} \quad (15)$$

In which the coefficients $B_1, B_2, B_3, M_1, M_2, M_3, T_1, T_2, T_3, A_1, A_2, A_3$ and A_4 are represented in the table below.

Table 1: Coefficients resulting from non dimensionalisation

	U_*	B_1	B_2	B_3	M_1	M_2
		$\frac{P_c}{\rho_c U_2^2}$	$\frac{gL_c}{U^2}$	$\frac{\mu_R}{\rho_R U, L_R}$	$\frac{P_c}{C_{Ppc}\Delta_c \Delta T_1}$	$\frac{\lambda_c}{\lambda_{P_c \rho_c U I_c}}$
Scheme	$\sqrt{g\beta\Delta T L_c}$	$\frac{EU \cdot F_c}{\zeta\eta}$	$\frac{1}{\zeta\eta}$	$\frac{1}{\sqrt{G_r}}$	$E_\mu E_C$	$\frac{1}{P_r\sqrt{G_r}}$

	M_3	T_1	T_2	T_3	A_1	A_2	A_3	A_4

		$\frac{\mu_c}{\rho_c U L_c}$	$\frac{gL_c}{U,2}$	$\frac{P_r}{\rho_c U^2}$	$\frac{\mu_c}{\rho_c U_c L_c}$	$\frac{\mu_c P_c}{\rho_c^2 U L_c}$	$\left(\frac{p_c - L_c}{\rho_c U_c L_c}\right)^2$	$\frac{g\mu_c}{\rho U^3}$
Scheme	$E_c R_e^{-1}$	$\frac{1}{\sqrt{G_r}}$	$\frac{i}{\zeta\eta}$	$\frac{E_r F_r}{\zeta\eta}$	$\frac{1}{\sqrt{G_r}}$	$\frac{E_r}{\sqrt{G_r}}$	$\frac{\sqrt{G_r}}{\frac{1}{\sqrt{G_r}}}$	$\frac{Fr}{\sqrt{G}}$

$\frac{U_*}{gL_c} = Fr$ (Froude number); $\frac{\rho_R U_z L_c}{\mu_R} =$ Re (Reynolds - number) $\frac{P_c}{\rho_c U_*^2} = Eu$ (Euler number); $\frac{P_c}{\rho_c C_{PR} T_c} = Pn$ (Pressure number)

$(\mu_c g/\rho_c)/c_{pc} T_c = Gn$ (Gravity number); $\zeta = \frac{\Delta T_*}{T_c}$ (Non - dimensional temperature difference) $\frac{\rho_c^2 C_{pc} g \beta \Delta T_* L_c}{\mu_c K_c} =$ Ra (Rayleigh - number); $\eta = \beta_R T_c$

$\frac{Ra}{\Pr} = Gr$ (Grashof number); $\frac{U^2 c}{C_{pc}\Delta T_*} = Ec$ (Eckert - number)

$\frac{\mu_c C_{pc}}{\lambda_c} =$ Pr (Prandtl number)

IV. Mathematical Modeling

These unknown turbulent correlations include $\overline{\nabla \cdot \rho u' u'}$ and $\frac{\partial C_p T' u'}{\partial x_i}$ known as Reynolds stress equation and heat flux equation respectively, for which it is crucial to identify the essential connections and equations for determining these unknown turbulent correlations. In this study, model turbulence for a k-ε model with explicitly expressed boundary conditions has been used.

The resultant equations that regulate natural convection in an enclosure are presented below after applying the Bousinessq approximation and substituting them into the governing equations 11 to 15 in non-dimensional form; The equation for continuity, which is (11), is simplified as

$$\frac{\partial U_j}{\partial X_j} = 0 \tag{16}$$

The equation for the momentum (12) is:

$$\frac{\partial U_j}{\partial t} + \frac{\partial U_i U_j}{\partial x_j} = -\frac{B_1}{\rho_c}\frac{\partial P}{\partial x_i} - B_2 \Theta g_i + \frac{\partial}{\partial x_j}\left(B_3\left(\frac{\partial U_i}{\partial x_j} + \frac{\partial U_j}{\partial x_i}\right) - \overline{u_i u_j}\right) \tag{17}$$

Where $B_2 = (B_2)_{\text{old}}\, \beta_c \Delta T_*$ and the $(B_2)_{\text{old}}$ is shown in the table.

The energy equation (13) results into:

$$\frac{\partial \Theta}{\partial t} + \frac{\partial}{\partial x_j} U_j \Theta = \frac{\partial}{\partial x_j}\left(M_2 \frac{\partial \Theta}{\partial x_j} - \overline{u_j \theta}\right) \tag{18}$$

The turbulent kinetic k becomes

$$\frac{\partial k}{\partial t} + \frac{\partial}{\partial x_j} U_j k = T_1 \overline{u_j \frac{\partial}{\partial x_j} v\left(\frac{\partial u_i}{\partial x_j} + \frac{\partial u_j}{\partial x_i}\right)} - \frac{\partial}{\partial x_j}\overline{u_j\left(\frac{u_i u_j}{2} + \frac{P}{\rho}\right)} + P_k + T_2 G_k \tag{19}$$

Where $P_k = -\overline{u_i' u_j'}\frac{\partial_j}{\partial x_i}$ and $G_k = \overline{\rho u_i}\frac{g_i}{\rho}$

The energy dissipation equation becomes

$$\frac{\partial \varepsilon}{\partial t} + \frac{\partial}{\partial x_j} U_j \varepsilon = -\frac{\partial}{\partial x_k}\left(\overline{A_1 v u_k \frac{\partial u_i}{\partial x_j}\frac{\partial u_k}{\partial x_j}} + A_2 v \overline{\frac{\partial u_k}{\partial x_i}\frac{\partial P}{\partial x_i}} - A_1 v \frac{\partial \varepsilon}{\partial x_k}\right) - 2A_1 v \overline{\frac{\partial u_t}{\partial x_j}\frac{\partial u_i}{\partial x_j}\frac{\partial u_k}{\partial x_j}} -$$
$$2A_3\left(\overline{v\frac{\partial^2 u_i}{\partial x_k \partial x_j}}\right)^2 + 2A_4 \frac{v}{\rho}\frac{\partial u_i}{\partial x_j}\frac{\partial P}{\partial x_j}\frac{\partial x_i}{g_i} - 2A_1 v \frac{\partial u_i}{\partial x_k}\left(\overline{\frac{\partial u_i}{\partial x_j}\frac{\partial u_k}{\partial x_j}} + \overline{\frac{\partial u_j}{\partial x_i}\frac{\partial u_j}{\partial x_k}}\right) - 2A_1 v \frac{\partial^2 u_i}{\partial x_j \partial x_k}\overline{U_k \frac{\partial u_i}{\partial x_j}} \tag{20}$$

Turbulent Stresses $\overline{u_i' u_j'}$ a and heat flux $\overline{u_j \theta}$ in turbulent flows are calculated as below

$$-\overline{u_i' u_j'} = v_t\left(\frac{\partial u_i}{\partial x_j} + \frac{\partial u_j}{\partial x_i}\right) - \frac{2}{3}k\delta_{ij}$$

And

$$\overline{u_j \theta} = -\frac{v_t}{\sigma T}\frac{\partial \Theta}{\partial x_j}$$

For which the v_t for $k - \varepsilon$ model is given by

$$v_t = c_\mu \frac{k^2}{\varepsilon}$$

Vorticity Vector Formulation

A combination of vorticity stream function and vector potential has been considered as a vorticity vector formulation in this study. The formulation has been used to eliminate the pressure term from the Navier Stokes since calculation velocities and pressures simultaneously using interpolation of equal orders is impossible. Thus for efficient numerical solution we have employed vorticity stream function. The dimensionless form of continuity equation 16 and 17 are reduced to

$$\frac{\partial U}{\partial X}+\frac{\partial V}{\partial Y}=0 \tag{21}$$

Momentum equation in x coordinates becomes

$$\frac{\partial U}{\partial t}+U\frac{\partial U}{\partial x}+V\frac{\partial U}{\partial y}=-\frac{B_1}{\rho_c}\frac{\partial P}{\partial x}-B_2\theta\cos\gamma+\frac{\partial}{\partial x}\left((B_3+v_t)2\frac{\partial U}{\partial x}-\frac{2}{3}k\right)+\frac{\partial}{\partial y}\left((B_3+v_t)2\frac{\partial U}{\partial y}+\frac{\partial V}{\partial x}\right) \tag{22}$$

Momentum equation in y coordinates becomes

$$\frac{\partial V}{\partial t}+U\frac{\partial V}{\partial x}+V\frac{\partial U}{\partial y}=-\frac{B_1}{\rho_c}\frac{\partial P}{\partial x}-B_2\Theta\sin\gamma+\frac{\partial}{\partial y}\left((B_3+v_t)\frac{\partial V}{\partial x}+\frac{\partial U}{\partial y}\right)+\frac{\partial}{\partial y}\left((B_3+v_t)2\frac{\partial V}{\partial y}-\frac{2}{3}k\right) \tag{23}$$

γ represents the angle between the gravitational vector and the x-axis. Velocity parameters are defined by stream function ψ (x, y,). as

$$U=\frac{\partial\psi}{\partial y}$$

$$V=-\frac{\partial\psi}{\partial x}$$

The momentum equations in x and y coordinates (4.4.2) and (4.4.3) are merged together by introducing vorticity vector ξ, which [15] defined as the curl$\vec{}$V and where $\vec{}$Vis the velocity vector. The connection between Stream function and vorticity vector is given by

$$\xi=\frac{\partial V}{\partial x}-\frac{\partial U}{\partial y} \tag{24}$$

and $$\frac{\partial^2\psi}{\partial x^2}+\frac{\partial^2\psi}{\partial y^2}=-\xi \tag{25}$$

The pressure factor is removed from the momentum equations by cross differentiating equations (21) and (22) with respect to y and x, respectively, and getting the difference between the resulting equations while considering the definition of vorticity equation (24). The parabolic vorticity transport equation is the resultant equation below:

$$\begin{aligned}\frac{D\xi}{Dt}&=(B_3+v_t)\nabla^2\xi+2\left(\frac{\partial v_t}{\partial x}\frac{\partial\xi}{\partial x}+\frac{\partial v_t}{\partial y}\frac{\partial\xi}{\partial y}\right)-(\nabla^2 v_t)\xi+2\left(\frac{\partial^2 v_t}{\partial x^2}\frac{\partial V}{\partial x}-\frac{\partial^2 v_t}{\partial y^2}\frac{\partial U}{\partial y}+2\frac{\partial^2 v_t}{\partial x\,\partial y}\frac{\partial V}{\partial y}\right)\\&-B_2\left(\frac{\partial\Theta}{\partial x}\sin\gamma-\frac{\partial\Theta}{\partial y}\cos\gamma\right)\end{aligned} \tag{26}$$

Three-dimensional flow using a vector potential formulation

Since vorticity flow function formulation is only valid for two-dimensional flow issues, we introduce a solenoidal vector field with a vector potential denoted by ψ = ψ$\vec{}$ = U$\vec{}$ i +V$\vec{}$ j +W$\vec{}$k. For vector potential ψ is defined as U = ∇ × ψ. And the equation relating the stream function to the vorticity is given as

$$\xi=-\nabla 2\psi \tag{27}$$

As a result, we obtain the three-dimensional vorticity equation as

$$\frac{\partial^2\psi_1}{\partial x^2}+\frac{\partial^2\psi_1}{\partial y^2}+\frac{\partial^2\psi_1}{\partial z^2}=-\xi_1,\frac{\partial^2\psi_2}{\partial x^2}+\frac{\partial^2\psi_2}{\partial y^2}+\frac{\partial^2\psi_2}{\partial z^2}=-\xi_2,\frac{\partial^2\psi_3}{\partial x^2}+\frac{\partial^2\psi_3}{\partial y^2}+\frac{\partial^2\psi_3}{\partial z^2}=-\xi_3 \tag{28}$$

The momentum equation written as a vector potential of vorticity, avoids the need for the pressure and primitive variables that we saw the three components of vorticity vector ξ are

$$\xi_1=\frac{\partial W}{\partial y}-\frac{\partial V}{\partial z},\xi_2=-\left(\frac{\partial W}{\partial x}-\frac{\partial U}{\partial z}\right),\xi_3=\frac{\partial V}{\partial x}-\frac{\partial U}{\partial y} \tag{29}$$

The curl of the momentum equation (17) is thus utilized to produce vorticity transport equations below

$$\begin{aligned}&\frac{\partial\xi_1}{\partial t}+U\frac{\partial\xi_1}{\partial x}+V\frac{\partial\xi_1}{\partial y}+W\frac{\partial\xi_1}{\partial z}-\xi_1\frac{\partial U}{\partial x}-\xi_2\frac{\partial U}{\partial y}-\xi_3\frac{\partial U}{\partial z}=(B_3+v_t)\nabla^2\xi_1+\frac{\partial v_t}{\partial x}\frac{\partial\xi_1}{\partial x}+2\frac{\partial v_t}{\partial y}\frac{\partial\xi_1}{\partial y}+2\frac{\partial v_t}{\partial z}\frac{\partial\xi_1}{\partial z}-\\&\frac{\partial v_t}{\partial y}\frac{\partial\xi_2}{\partial x}-\frac{\partial v_l}{\partial z}\frac{\partial\xi_3}{\partial x}-\left(\frac{\partial^2 v_t}{\partial y^2}+\frac{\partial^2 v_t}{\partial z^2}\right)\xi_1+\frac{\partial^2 v_t}{\partial x\,\partial y}\xi_2+\frac{\partial^2 v_f}{\partial x\,\partial z}\xi_3+2\left[\frac{\partial^2 v_z}{\partial x\,\partial y}\frac{\partial W}{\partial x}+\frac{\partial^2 v_r}{\partial y^2}\frac{\partial W}{\partial y}+\frac{\partial^2 v_z}{\partial y\,\partial z}\frac{\partial W}{\partial z}-\left(\frac{\partial^2 v_1}{\partial x\,\partial z}\frac{\partial V}{\partial x}+\right.\right.\\&\left.\left.\frac{\partial^2 v_l}{\partial y\,\partial z}\frac{\partial V}{\partial y}+\frac{\partial^2 v_z}{\partial z^2}\frac{\partial V}{\partial z}\right)\right]\end{aligned} \tag{30}$$

$$\begin{aligned}&\frac{\partial\xi_2}{\partial t}+U\frac{\partial\xi_2}{\partial x}+V\frac{\partial\xi_2}{\partial y}+W\frac{\partial\xi_2}{\partial z}-\xi_1\frac{\partial V}{\partial x}-\xi_2\frac{\partial V}{\partial y}-\xi_j\frac{\partial V}{\partial z}=(B_3+v_2)\nabla^2\xi_2+2\frac{\partial v_1}{\partial x}\frac{\partial\xi_2}{\partial x}+\frac{\partial v_1}{\partial y}\frac{\partial\xi_2}{\partial y}+2\frac{\partial v_y}{\partial z}\frac{\partial\xi_2}{\partial z}-\\&\frac{\partial v_l}{\partial x}\frac{\partial\xi_1}{\partial y}-\frac{\partial v_1}{\partial z}\frac{\partial\xi_3}{\partial y}-\left(\frac{\partial^2 v_l}{\partial x^2}+\frac{\partial^2 v_l}{\partial z^2}\right)\xi_2+\frac{\partial^2 v_t}{\partial x\,\partial y}\xi_1+\frac{\partial^2 v_l}{\partial y\,\partial z}\xi_3-B_3\frac{\partial\Theta}{\partial z}+2\left[\frac{\partial^2 v_l}{\partial x\,\partial z}\frac{\partial U}{\partial x}+\frac{\partial^2 v_t}{\partial y\,\partial z}\frac{\partial W}{\partial y}+\frac{\partial^2 v_t}{\partial z^2}\frac{\partial U}{\partial z}-\left(\frac{\partial^2 v_t}{\partial x^2}\frac{\partial W}{\partial x}+\right.\right.\end{aligned}$$

$\frac{\partial^2 v_I}{\partial x\,\partial y}\frac{\partial W}{\partial y}+\frac{\partial^2 v_I}{\partial x\,\partial z}\frac{\partial W}{\partial z}\Big)\Big]$ (31)

$\frac{\partial \xi_3}{\partial t}+U\frac{\partial \xi_3}{\partial x}+V\frac{\partial \xi_3}{\partial y}+W\frac{\partial \xi_3}{\partial z}-\xi_1\frac{\partial W}{\partial x}-\xi_2\frac{\partial W}{\partial y}-\xi_3\frac{\partial W}{\partial z}=(B_3+v_t)\nabla^2\xi_3+2\frac{\partial v_l}{\partial x}\frac{\partial \xi_3}{\partial x}+2\frac{\partial v_1}{\partial y}\frac{\partial \xi_3}{\partial y}+\frac{\partial v_t}{\partial z}\frac{\partial \xi_3}{\partial z}-\frac{\partial v_r}{\partial x}\frac{\partial \xi_1}{\partial z}-\frac{\partial v_t}{\partial y}\frac{\partial \xi_2}{\partial z}-\left(\frac{\partial^2 v_t}{\partial x^2}+\frac{\partial^2 v_t}{\partial y^2}\right)\xi_3+\frac{\partial^2 v_t}{\partial x\,\partial z}\xi_1+\frac{\partial^2 v_t}{\partial y\,\partial z}\xi_2-B_2\frac{\partial \Theta}{\partial y}+2\left[\frac{\partial^2 v_t}{\partial x^2}\frac{\partial V}{\partial x}+\frac{\partial^2 v_t}{\partial x\,\partial y}\frac{\partial V}{\partial y}+\frac{\partial^2 v_l}{\partial x\,\partial z}\frac{\partial V}{\partial z}-\left(\frac{\partial^2 v_y}{\partial x\,\partial y}\frac{\partial U}{\partial x}+\frac{\partial^2 v_y}{\partial y^2}\frac{\partial U}{\partial y}+\frac{\partial^2 v_1}{\partial y\,\partial z}\frac{\partial U}{\partial z}\right)\right]$ (32)

The vorticity transport equations (30), (31), and (32), as well as the vorticity equation (28), are used to replace the continuity and momentum equations given by equations (16), (17) and (18). The variables to be solved includes; ξ1, ξ2, ξ3, U, V, W, Θ. The k and ε are determined by making use of the equations for turbulent energy that Ince and Launde derived in 1989, which are as follows.;

$\frac{\partial k}{\partial t}+\frac{\partial}{\partial x_j}U_j k=v_I\left(\frac{\partial U_i}{\partial x_j}+\frac{\partial U_j}{\partial x_j}\right)\frac{\partial U_i}{\partial x_j}-\varepsilon+\frac{\partial}{\partial x_j}\left[\left(T_2+\frac{v_t}{\sigma_k}\right)\frac{\partial k}{\partial x_j}\right]-T_2 g_i\overline{u_\iota\theta}$ (33)

$\frac{\partial \bar{\varepsilon}}{\partial t}+\frac{\partial}{\partial x_j}U_j\underline{\varepsilon}=C_{r1}\frac{\varepsilon}{k}v_i\left(\frac{\partial U_j}{\partial x_j}+\frac{\partial U_j}{\partial x_i}\right)\frac{\partial U_i}{\partial x_j}-C_{r2}\frac{\varepsilon^2}{k}+2F_1^2 v_i\left(\frac{\partial^2 U_j}{\partial x_j\,\partial x_k}\right)^2+\frac{\partial}{\partial x_j}\left[\left(F_1+\frac{v_2}{\sigma_\varepsilon}\right)\frac{\partial \bar{\varepsilon}}{\partial x_i}\right]+F_4 g_i\overline{U_\iota\theta}\frac{\bar{\varepsilon}}{k}+0.83\left(\frac{k^{\frac{3}{2}}}{\varepsilon C_1 x_n}-1\right)^2\frac{\varepsilon^2}{k}$ (34

Where

$\varepsilon=\bar{\varepsilon}+D$ and $D=2v\left(\frac{\partial k^1}{\partial x_j}\right)^2$

Boundary Conditions

Velocity Boundary Conditions

Velocity is a unit used to indicate the conditions for fluid movement at a barrier. We utilize a no slip boundary condition, stating that a viscous fluid's velocity with regard to a solid boundary is zero. As the fluid travels, the molecules are thought to have a larger adhesive force than cohesive force. In a closed hollow, every barrier is impermeable and only travels in that direction. This means that the normal velocity component is 0 at all boundaries. An impermeable solid surface cannot permit mass to pass through it, hence, considering the X-Y plane, the surface velocity component is always zero since X = 0.

Temperature Boundary Conditions

The equation $\Theta=\frac{T-\tau_*}{\Delta T_+}$ provides the definition of the temperature in a non-dimensional form. The temperature difference between warm and cool surfaces, denoted by ΔT_* That is $\Delta T_*=T_h-T_c$, where the selection of ΔT, guarantees that it is constrained and ranges from 0 to 1. The following equations reflect the isothermal and adiabatic boundary conditions for heat flow, respectively.

$\Delta T_*=$ Constant

$\frac{\partial \Theta}{\partial n}=0$

Where n indicates the wall's perpendicularity. The other four walls of the enclosure are kept in an adiabatic state since the core problem requires cooling on one wall and heating on the other. The Dirichlet boundary conditions are implemented as follows on the hot and cold walls.

$\Theta_{\text{her}}=1$ and $\Theta_{cold}=0$ while the Neumann boundary conditions are applied to the remaining four walls such as $\frac{\partial \Theta}{\partial n}=0$.

Vector Potential Boundary Condition

On the non-slip edge, the contour conditions are challenging. The tangential components on the surface and the normal derivatives of the normal component are the only ψ components that are not completely zero. For instance, considering the wall along the y-z level where $X=0$ we have $\frac{\partial \psi_1}{\partial x},\psi_2=\psi_3=0$. In the same way, along the $x-z$ level at $Y=0$ we have $\frac{\partial \psi_2}{\partial y},\psi_1=\psi_3=0$ and on $x-y$ level at $Z=0$, $\frac{\partial \psi_1}{\partial z},\psi_1=\psi_2=0$.

In our investigation, several Rayleigh numbers were used to produce the results, but the aspect ratios remained fixed at 2. The opposite cold wall is maintained at 288 K, while the hot wall is maintained at 308 K. While the other walls are kept adiabatic, the enclosure operates at a temperature of 298 K.

Vorticity Boundary Conditions

Equation (27), produces the boundary conditions for vorticity. The equation's fundamental velocities can be used to express the elements of the no-slip vorticity (29). Taking into account the y-z boundary. where $\frac{\partial W}{\partial y} = \frac{\partial V}{\partial z} = \frac{\partial U}{\partial z} = \frac{\partial U}{\partial y} = 0$, by application of right hand rule the vorticity boundary becomes $\xi_1 = 0, \xi_2 = -\frac{\partial w}{\partial x}, \xi_3 = \frac{\partial y}{\partial x}$.

Similarly, the wall along the $x - y$ level where$\frac{\partial U}{\partial y} = \frac{\partial V}{\partial x} = \frac{\partial W}{\partial x} = \frac{\partial W}{\partial y} = 0$ giving vorticity boundary conditions of $\xi_1 = -\frac{\partial y}{\partial z}, \xi_2 = \frac{\partial U}{\partial z}, \xi_3 = 0$. For the wall along the $x - z$ level, we have $\frac{\partial W}{\partial x} = \frac{\partial U}{\partial z} = \frac{\partial V}{\partial z} = \frac{\partial V}{\partial x} = 0$, resulting to$\xi_1 = \frac{\partial W}{\partial y}, \xi_2 = 0, \xi_3 = -\frac{\partial U}{\partial y}$.

Table 2: Turbulence Coefficients.

$C_{1\varepsilon}$	$C_{2\varepsilon}$	C_{μ}	σ_{ϵ}	σ_k
1.44	1.92	0.09	1.3	1.0

V. Numerical Methods

With the assistance of the finite difference approach, we are able to determine the solutions to the systems of nonlinear partial differential equations, coupled with their boundary conditions. To get an approximation of the partial differential equations in this scenario, we solve a set of linear equations that are based on the values of the functions at each mesh position. Due to the non-linear nature of these partial differential equations, an iterative method is required; the false transient method is an excellent choice for this particular application. [16]developed a method known as the false transient method, which adds false transient derivatives which is the process of transforming an equation into its parabolic equivalent. If a steady-state solution is sufficient, then the transient terms in the equations can be eliminated.

False Transient Method

In this strategy, transitory fictitious components $\frac{1}{\beta\theta}$ is added to the mean energy equation's time derivative, (18), $\frac{1}{\beta_3}$ is added to the vorticity transport equations,(30), (31), and (32), Both the turbulent kinetic energy equation (33) and the turbulent kinetic energy dissipation equation (34) are modified by the addition of $\frac{1}{\beta_k}$ and $\frac{1}{\beta_\varepsilon}$, respectively. The coefficients $\beta_\Theta, \beta_\xi, \beta_k$ and β_ε are useful for establishing the right time step for the solution as well as enabling for speedier solution convergence. For estimating the differential equations, a mesh grid that works well must be chosen. In this way, the solution space is partitioned into rectangular volume elements, which, individually, stand in for volumes of depth one and are centred on respective mesh nodes, and whose coordinates are expressed in form of the integer variables i, j and k

Finite Difference Approximations

The approach of approximation employing central, forward, and backward differences is utilized correctly; for example, we use backward and forward differences at corners and near edges. The convective term is approximated using a hybrid differentiation technique that blends central and upwind patterns. In addition, non-uniform grids have been employed because convective terms are predominant. The spacing of the grid varies over the solution volume. Thus, parts with higher flow gradients use smaller spacing, while parts with lower flow gradients use larger distances.

Mesh Points

Natural turbulent convection flow in a structure is characterized by a thermally stratified center and a thin boundary layer around the walls. The border layer has very substantial flow gradients that call for large number of lattice points. In this case study, the enclosure's domain of the solution is divided into a network of uniform rectangular grids of 60 by 50 meshes with very fine spacing as shown below

Figure 1: 60 by 50 Mesh points are represented as below,

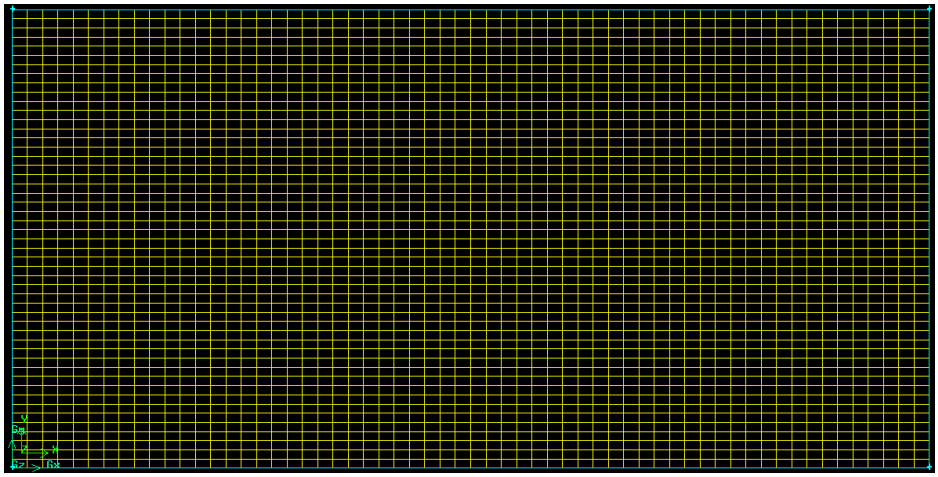

Figure 2: Mesh points

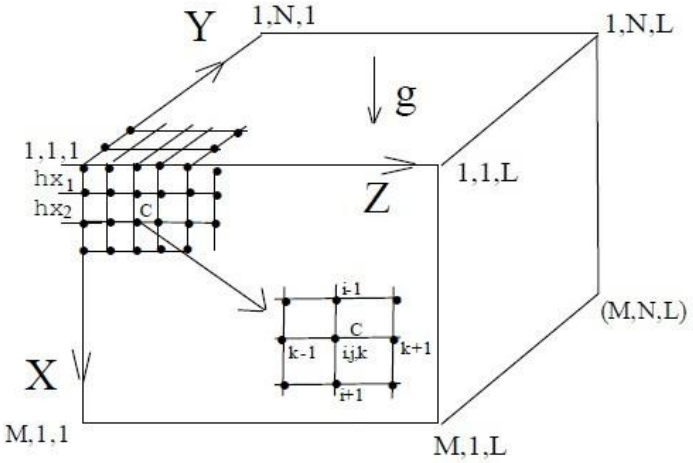

Figure 3: Nodes and elements

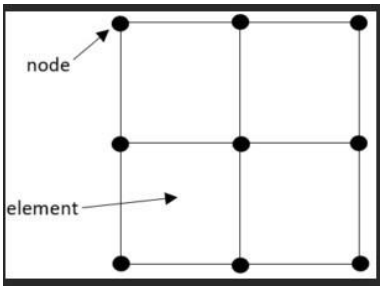

After utilizing the finite difference approximation for PDEs, the following mesh point variables are recorded: $\emptyset = \emptyset(i,j,k)$

$\emptyset(i-1) = \emptyset(i-1,j,k)$ (35)

Differentials at mesh locations are given by,

$$\frac{\partial \emptyset}{\partial x} = \frac{h_i^2}{h_i^2 h_{i+1} + h_i h_{i+1}^2}\emptyset_{i+1} + \frac{-(h_i^2 + h_{i+1}^2)}{h_i^2 h_{i+1} + h_i h_{i+1}^2}\emptyset + \frac{-h_{i+1}^2}{h_i^2 h_{i+1} + h_i h_{i+1}^2}\emptyset_{i-1} \quad (36)$$

$$\frac{\partial \emptyset}{\partial y} = \frac{h_j^2}{h_j^2 h_{j+1} + h_j h_{j+1}^2}\emptyset_{j+1} + \frac{-\left(h_j^2 + h_{j+1}^2\right)}{h_j^2 h_{j+1} + h_j h_{j+1}^2}\emptyset + \frac{-h_{j+1}^2}{h_j^2 h_{j+1} + h_j h_{j+1}^2}\emptyset_{j-1} \quad (37))$$

$$\frac{\partial \emptyset}{\partial z} = \frac{h_k^2}{h_k^2 h_{k+1} + h_k h_{k+1}^2}\emptyset_{k+1} + \frac{-(h_k^2 + h_{k+1}^2)}{h_k^2 h_{k+1} + h_k h_{k+1}^2}\emptyset + \frac{-h_{k+1}^2}{h_k^2 h_{k+1} + h_k h_{k+1}^2}\emptyset_{k-1} \quad (38)$$

The second derivatives are given as below;

$$\frac{\partial^2 \emptyset}{\partial x^2} = \frac{2h_i}{h_i^2 h_{i+1} + h_i h_{i+1}^2}\emptyset_{i+1} + \frac{-2(h_i + h_{i+1})}{h_i^2 h_{i+1} + h_i h_{i+1}^2}\emptyset + \frac{2h_{i+1}}{h_i^2 h_{i+1} + h_i h_{i+1}^2}\emptyset_{i-1} \quad (39)$$

$$\frac{\partial^2 \emptyset}{\partial y^2} = \frac{2h_j}{h_j^2 h_{j+1} + h_j h_{j+1}^2}\emptyset_{j+1} + \frac{-2\left(h_j + h_{j+1}\right)}{h_j^2 h_{j+1} + h_j h_{j+1}^2}\emptyset + \frac{2h_{j+1}}{h_j^2 h_{j+1} + h_j h_{j+1}^2}\emptyset_{j-1} \quad (40)$$

$$\frac{\partial^2 \emptyset}{\partial z^2} = \frac{2h_k}{h_k^2 h_{k+1} + h_k h_{k+1}^2}\emptyset_{k+1} + \frac{-2(h_k + h_{k+1})}{h_k^2 h_{k+1} + h_k h_{k+1}^2}\emptyset + \frac{2h_{k+1}}{h_k^2 h_{k+1} + h_k h_{k+1}^2}\emptyset_{k-1} \quad (41)$$

We use the following designations to simplify the equations on the x-axis.

$$D1_x = \frac{2h_i}{h_i^2 h_{i+1} + hh_i^2 h_{i+1}}$$

$$D2_x = \frac{-\left(h_i^2 + h_{j+1}^2\right)}{h_i^2 h_{i+1} + h_i h_{i+1}^2}$$

$$D3_x = \frac{-h_{i+1}^2}{h_i^2 h_{i+1} + h_i h_{i+1}^2}$$

$$D4_x = \frac{2h_i}{h_i^2 h_{i+1} + h_i h_{i+1}^2}$$

$$D5_x = \frac{-2(h_i + h_{i+1})}{h_i^2 h_{i+1} + h_i h_{i+1}^2}$$

$$D6_x = \frac{2h_{i+1}}{h_i^2 h_{i+1} + h_i h_{i+1}^2}$$

The equations in the y-and z-axes are then simplified with the help of the corresponding indices Thus equation (36) and (39) reduces to, $\frac{\partial \emptyset}{\partial x} = D1_x \vartheta_{i+1} + D2_x \vartheta + D3_x \vartheta_{i-1}$ and $\frac{\partial^2 \emptyset}{\partial x^2} = D4_x \emptyset_{i+1} + D5_x \theta + D6_x \theta_{i-1}$.

The application of these on equation (18), (30) (32), (33) and (34) are used to derive the finite difference equations, the steps below are then taken.

Mean equation energy equation (18) becomes:

$$\frac{\Theta^{n+1} - \Theta}{\beta_\Theta \Delta t} = -U(D1_x\Theta_{i-1} + D2_x\Theta + D3_x\Theta_{i+1}) - V\left(D1_y\Theta_{j-1} + D2_y\Theta + D3_y\Theta j_{j+1}\right) - W\left(D1_z\Theta_{K-1} + D2_y\Theta + D3_z\Theta_{K+1}\right) + \left(M_2 + \frac{v_t}{\sigma_j}\right)\left(D4_x\Theta_{i-1} + D5_x\Theta + D6_x\Theta_{i+1} + D4_y\Theta_{j-1} + \left(D5_y\Theta + D6_y\Theta_{j+1} + D4_z\Theta_{k-1} + D5_z\Theta + D6_y\Theta_{k+1}\right) + \frac{1}{\sigma_T}\left[\left(D1_x v_{t_t-1} + D2_x v_t + \right).\left(D3_x v_{t_{i+1}}\right)(D1_x\Theta_{i-1} + D2_x\Theta + D3_x\Theta_{i+1}) + \left(D1_y v_{t_{j-1}} + D2_y v_t + D3_y v_{t_{j+1}}\right)\left(D1_y\Theta j_{j-1} + \right)\left(D2_y\Theta + D3_y\Theta_{j+1}\right) + \left(D1_z v_{t_{k-1}} + D2_z v_t + D3_z v_{t_{k+1}}\right)(D1_z\Theta_{k-1} + D2_z\Theta + D3_z\Theta_{k+1})\right] \quad (42)$$

Where $M_2 = \frac{1}{P_r\sqrt{G_r}}$

Velocity equations are as follows:

$$U = D1_y\psi_{3j-1} + D2_y\psi_3 + D3_y\psi_{3j+1} - (D1_z\psi_{2k-1} + D2_z\psi_2 + D3_z\psi_{2k+1}) \quad (43)$$

$$V = D1_z\psi_{1k-1} + D2_z\psi_1 + D3_z\psi_{3k+1} - (D1_x\psi_{3i-1} + D2_x\psi_3 + D3_x\psi_{3i+1}) \quad (44)$$

$$W = D1_x\psi_{2i-1} + D2_x\psi_2 + D3_x\psi_{3i+1} - \left(D1_y\psi_{1j-1} + D2_y\psi_1 + D3_y\psi_{1j+1}\right) \quad (45)$$

Vector potential equations resulting from (28) are as follows:

$$D4_x\psi_{1i-1} + D5_x\psi_1 + D6_x\psi_{1i+1} + D4_y\psi_{1j-1} + D5_y\psi_1 + D6_y\psi_{1j+1} + D4_z\psi_{1k-1} + D5_z\psi_1 + D6_z\psi_{1k+1} = -\xi_1$$
$$D4_x\psi_{2i-1} + D5_x\psi_1 + D6_x\psi_{2i+1} + D4_y\psi_{2j-1} + D5_y\psi_2 + D6_y\psi_{2j+1} + D4_z\psi_{2k-1} + D5_z\psi_2 + D6_z\psi_{2k+1} = -\xi_2$$
$$D4_x\psi_{3i-1} + D5_x\psi_3 + D6_x\psi_{3i+1} + D4_y\psi_{3j-1} + D5_y\psi_3 + D6_y\psi_{1j+1} + D4_z\psi_{3k-1} + D5_z\psi_3 + D6_z\psi_{3k+1} = -\xi_3$$

$$\frac{\xi_1^{n+1}-\xi_1}{\beta_\xi \Delta t} = -U(D1_x\xi_{1i-1} + D2_x\xi_1 + D3_x\xi_{1i+1}) - V\big(D1_y\xi_{1j-1} + D2_y\xi_1 + D3_y\xi_{1j+1}\big) - W(D1_z\xi_{1k-1} + D2_z\xi_1 + D3_z\xi_{1k+1}) + \xi_1(D1_xU_{i-1} + D2_xU + D3_xU_{i+1}) + \xi_2\big(D1_yU_{j-1} + D2_yU + D3_yU_{j+1}\big) + \xi_3(D1_zU_{k-1} + D2_zU + D3_zU_{k+1}) + (D3_xv_t)[D4_x\xi_{3i-1} + D5_x\xi_1 + D6_x\xi_{1i+1} + D4_y\xi_{1j-1} + D5_y\xi_1 + D6_y\xi_{1j+1} + D4_z\xi_{1k-1} + D5_z\xi_1 + D6_z\xi_{1k+1}] + (D1_xv_{ut-1} + D2_xv_t + D3_xv_{t+1})(D1_x\xi_{1i-1} + D2_x\xi_1 + D3_x\xi_{1t+1}) + 2\big(D1_yv_{tj-1} + D2_yv_l + D3_yv_{tj+1}\big)\big(D1_y\xi_{1j-1} + D2_y\xi_1 + D3_y\xi_{1j+1}\big) + 2(D1_zv_{tk-1} + D2_zv_t + D3_zv_{tk+2})(D1_z\xi_{1k-1} + D2_z\xi_1 + D3_z\xi_{1k+1}) - \big(D1_yv_{tj-1} + D2_yv_t + D3_yv_{tj+1}\big)(D1_x\xi_{2i-1} + D2_x\xi_2 + D3_x\xi_{2t+1}) - (D1_zv_{tk-1} + D2_zv_t + D3_zv_{kk+1})(D1_x\xi_{2i-1} + D2_x\xi_2 + D3_x\xi_{2t+1}) - \big(D4_yv_{tj-1} + D5_yv_t + D6_yv_{tj+1} + D4_zv_{tk-1} + D5_zv_l + D6_zv_{tk+1}\big)\xi_1 + \big[D1_y\big(D1_xv_{u-1,j-1} + D2_xv_{u,j-1} + D3_xv_{ui+1,j-1}\big) + D2_y\big(D1_xv_{ti-1} + D2_xv_fi + D3_xv_{ti+1}\big) + D3_y\big(D1_xv_{ti-1,j+1} + D2_xv_{t,j+1} + D3_xv_{ti+1,j+1}\big)\big]\xi_2 + \big[D1_z\big(D1_xv_{ti-1,k-1} + D2_xv_{t,k-1} + D3_xv_{ti+1,k-1}\big) + D2_z(D1_xv_{ti-1} + D2_xv_t + D3_xv_{ti+1}) + D3_z\big(D1_xv_{ti-1,k+1} + D2_xv_{ti+1} + D3_xv_{ti+1,k+1}\big)\big]\xi_3 + 2\{\big[D1_y\big(D1_xv_{ti-1,j-1} + D2_xv_{t,j-1} + D3_xv_{ti+1,j-1}\big) + D2_y\big(D1_xv_{ti-1,j-1} + D2_xv_{t,j-1} + D3_xv_{ti+1,j-1}\big)\big](D1_xW_{i-1} + D2_xW + D3_xW_{i+1}) + \big(D4_yv_{tj-1} + D5_yv_t + D6_yv_{tj+1}\big)(D1_xW_{i-1} + D2_xW + D3_xW_{i+1}) + \big[D1_z\big(D1_yv_{tj-1k-1} + D2_yv_{tk-1} + D3_yv_{tj+1k-1}\big) + D2_z\big(D1_yv_{tj-1} + D2_yv_l + D3_yv_{tj+1}\big) + D3_z\big(D1_yv_{t,j-1,k+1} + D2_yv_{tk+1} + D3_yv_{tj+1k+1}\big)\big](D1_xW_{i-1} + D2_xW + D3_xW_{i+1}) - \big[D1_z\big(D1_xv_{ti-1,k-1} + D2_xv_{t,k-1} + D3_xv_{t+1,k-1}\big) + D2_z\big(D1_yv_{ti-1} + D2_yv_t + D3_yv_{ti+1}\big) + D3_z(D1_xv_{ti-1k+1} + D2_xv_{tk+1} + D3_xv_{t,i+1,k+1})\big](D1_xV_{i-1} + D2_xV + D3_xV_{i+1}) + \big[D1_z\big(D1_yv_{tj-1,k-1} + D2_yv_{tk-1} + D3_yv_{tj+1k-1}\big) + D2_z\big(D1_yv_{tj-1} + D2_yv_t + D3_yv_{t,j+1}\big) + AZ3\big(D1_yv_{tj-1,k+1} + D2_yv_{tk+1} + D3_yv_{tj+1k+1}\big)\big(D1_yV_{j-1} + D2_yV + D3_yV_{j+1}\big)\big(D4_yV_{tk-1} + D5_yV_t + D6_yV_{tk+1}\big)\big(D1_yV_{k-1} + D2y + D3_yV_{k+1}\big)\big]\}$$

Turbulent flow essential input

Table no 3: The input of turbulent flow necessary to simulate and acquire the results of this study.

Input	Value	
Geometry		Aspect Ratio
Ra =1.552 x 1010	2 x 1 x 1	2
Ra =9.934 x 1011	8 x 4 x 4	2
Ra =1.552 x 1013	20 x 10 x 10	2
Ra =2.425 x 1014	50 x 25 x 25	2
Models		
Energy	On	
Viscous	Standard $k-\varepsilon$	
Material Properties at 298 K		
Density	1.1845kg/m3	
Dynamic Viscousity	1.8444E-05 Kg/ms	
Specific heat capacity	1.0063E+03 J/Kg/K	
Thermal Conductivity	0.025969 W/m.K	

Thermal Expansion coefficient	3.3540E-03 1/K
Prandtl number	0.7147
Gravitational force	9.81 m/s2
Solution models	
Pressure	PRESTO
Momentum	First Order Upwind
Turbulent Kinetic Energy	First Order Upwind
Turbulent Dissipation Rate	First Order Upwind

Table 2: Turbulent flow input

VI. RESULTS

Distribution of streamlines

A streamline is the path traced by a massless particle moving with the flow. Resistance to flow in fluids like air is minimized along these lines, which extend at right angles to the flow direction. For this study, the results were found for Rayleigh numbers between 1.522 × 1010 and 2.452 × 1014. The figures show how the streamlines are spread out, and they prove that two separate vortices are in motion. A vortex is defined as a swirling fluid motion. It has been noticed that as the Rayleigh number increases, so does the velocity, with the minimum being 1.30 × 10−1Kg/s and maximum being 2.53 × 101Kg/s. The movement of the streamlines originates from the hot wall. Thus, this conclusion is consistent with the idea of heat transfer. The buoyancy forces, the magnitude of the vortices, and the strength of the stream function all rise with the Rayleigh number. The results reported here agree with those from the experimental studies published by [17]

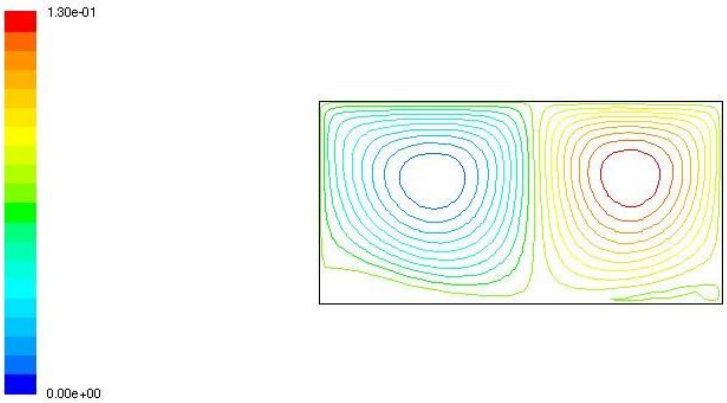

Figure 4: Streamline distribution for Ra = 1.552×10^{10}

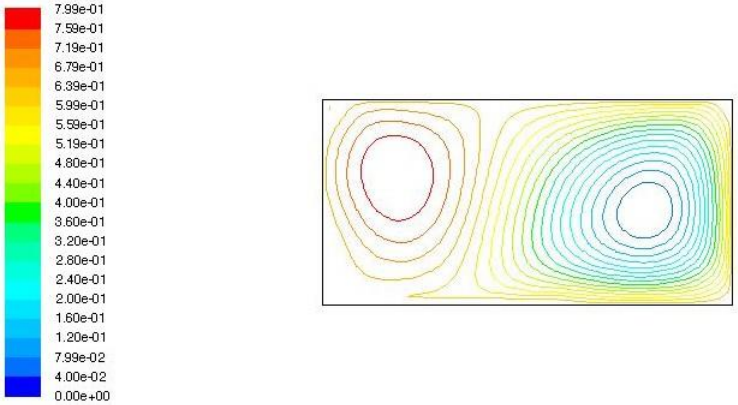

Figure 5: Streamline distribution for Ra = 9.934×11^{10}

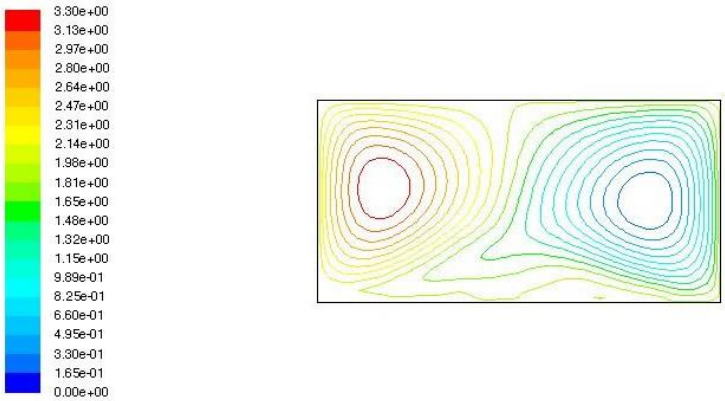

Figure 6: Streamline distribution for Ra = 1.552×10^{13}

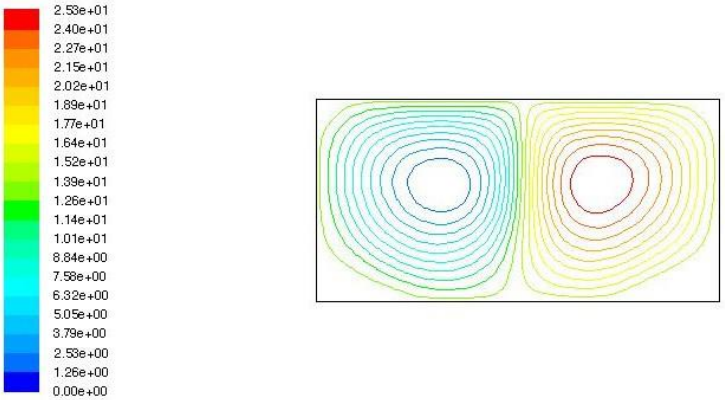

Figure 7: Streamline distribution for Ra = 2.425×10^{14}

Contours of Velocity magnitudes (m/s)

The figures below 8, 9, 10, 11 represents the contours of velocity magnitude. As the number of Rayleigh grows, there is a corresponding increase in the number of vortices. Furthermore, the streamlines on the heated wall grow as the number of Rayleigh rises. The flow becomes more chaotic with rising Rayleigh number, leading to a rise in velocity magnitude, as shown in figures 8 and 11, where a slowest velocity of 0.308 m/s was recorded and the maximum velocity was measured at 2.23 m/s, respectively. These findings are consistent with those of the practical investigational study by [17]which found that a higher Rayleigh number leads to a greater velocity

Figure 8: Contours of velocity magnitude for $Ra = 1.552 \times 10^{10}$

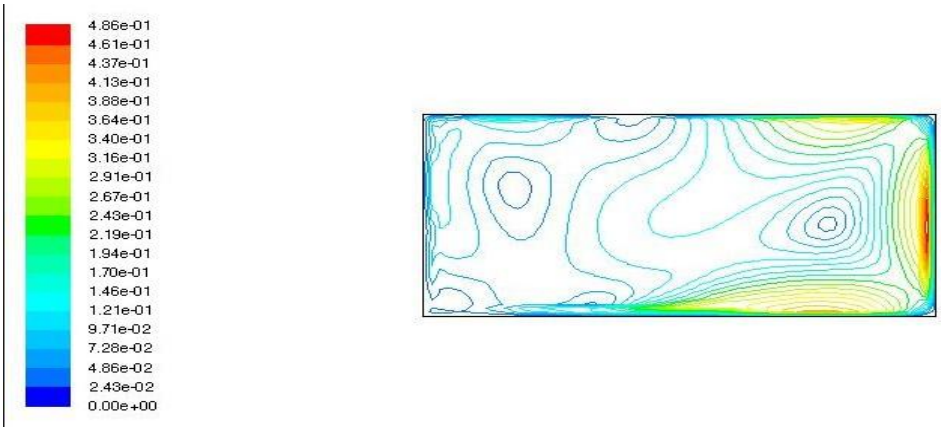

Figure 9: Contours of velocity magnitude for $Ra = 9.934 \times 10^{11}$

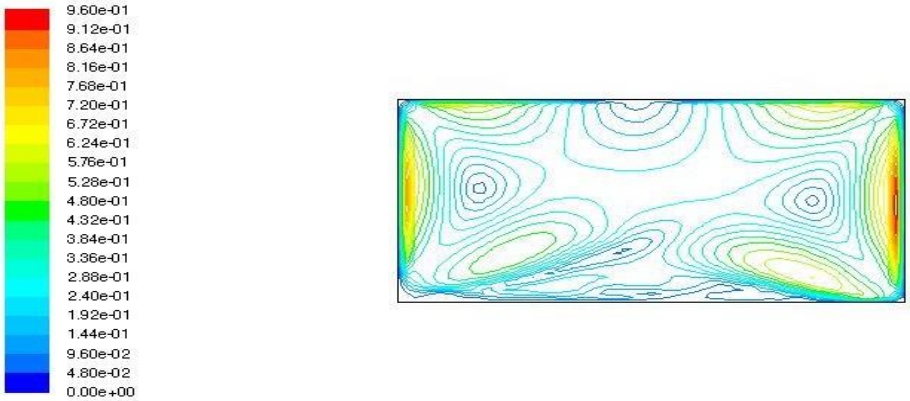

Figure 10: Contours of velocity magnitude for $Ra = 1.552 \times 10^{13}$

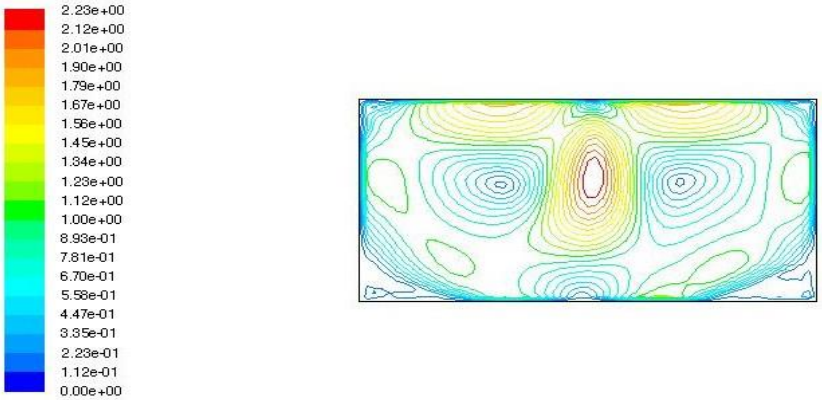

Figure 11: Contours of velocity magnitude for $Ra = 2.425 \times 10^{14}$

Contours of total temperature/Isotherms

The term "isotherm" refers to a line or curve on a temperature graph that joins two spots with the same temperature. Convection has a larger part in heat transfer as the Rayleigh number rises. It's clear that as the Rayleigh number rises, the maximum temperature falls. The highest temperature depicted is 290 degrees Kelvin in Figure 12, 288 degrees Kelvin in Figure 13, 282 degrees Kelvin in Figure 14, and 279 degrees Kelvin in Figure 15. The heat flow is portrayed as a series of contours that begin at the warm wall and terminate at the cool wall. It's also important to note that the buoyancy forces get stronger as the Rayleigh number goes up. This thins the thermal boundary layer along the hot wall and brings the hot spots closer to the centre. It is easy to see from the figures below how the Rayleigh number varies in relation to the overall temperature.

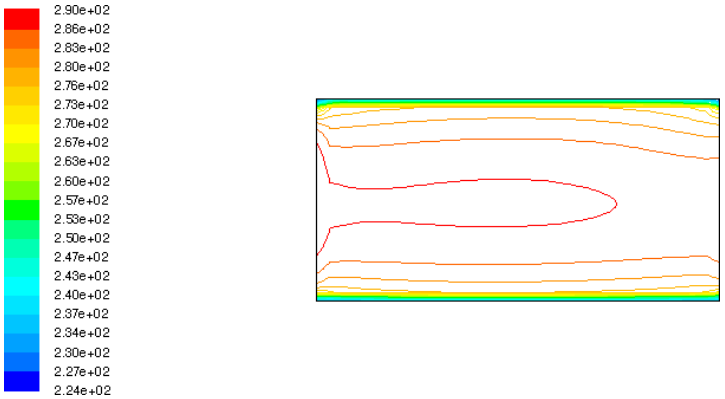

Figure 12: Contours of isotherms for $Ra = 1.552 \times 10^{10}$

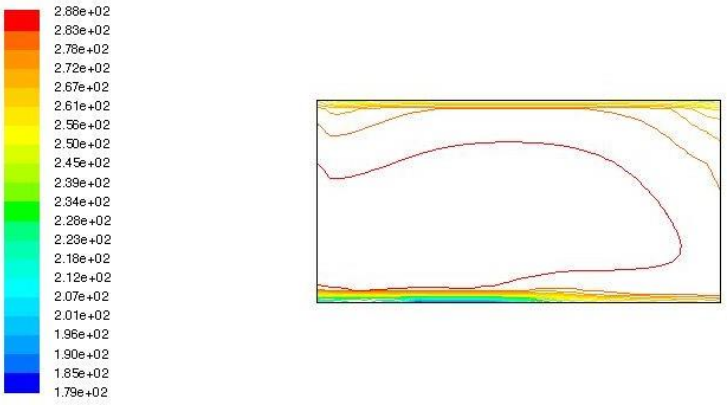

Figure 13: Contours of isotherms for $Ra = 9.934 \times 10^{11}$

Figure 14: Contours of isotherms for $Ra = 1.552 \times 10^{13}$

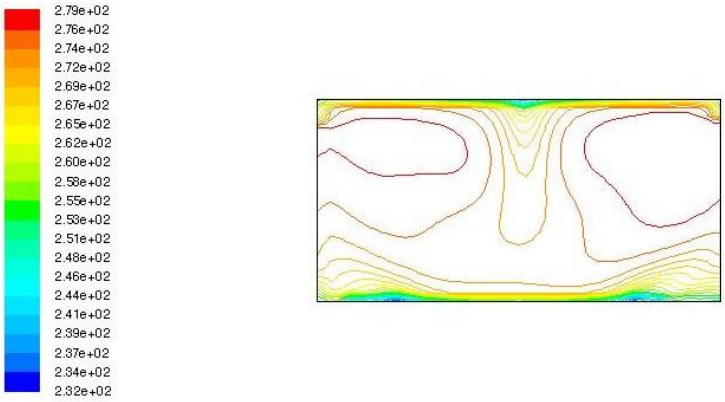

Figure 15: Contours of isotherms for $Ra = 2.425 \times 10^{14}$

Contours of Turbulent Kinetic Energy

For this purpose, the results reveal that the kinetic energy of the turbulent fluid increases as the Rayleigh number increases. The following diagrams illustrate this point perfectly. The kinetic energy fluctuations, and hence the fluid velocity inside the enclosure, increase with increasing Rayleigh number. It is also discovered that at high-velocity regimes close to the heated wall, the Rayleigh number has a major impact on the flow structure of turbulent kinetic energy. The top wall has more kinetic energy than the lower wall.

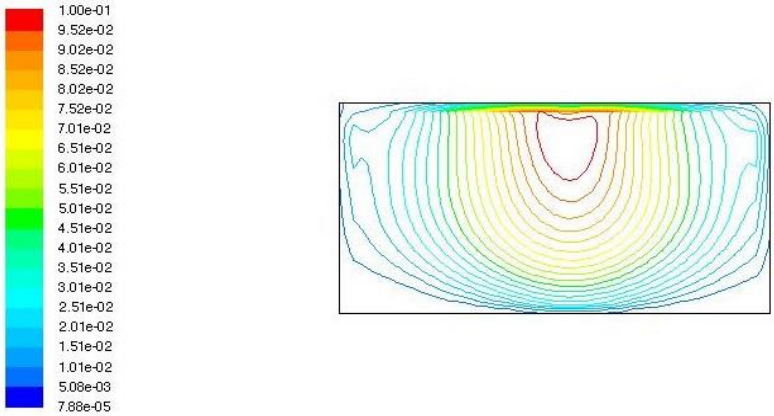

Figure 16: Contours of Turbulent Kinetic Energy for $\boldsymbol{Ra = 1.552 \times 10^{10}}$

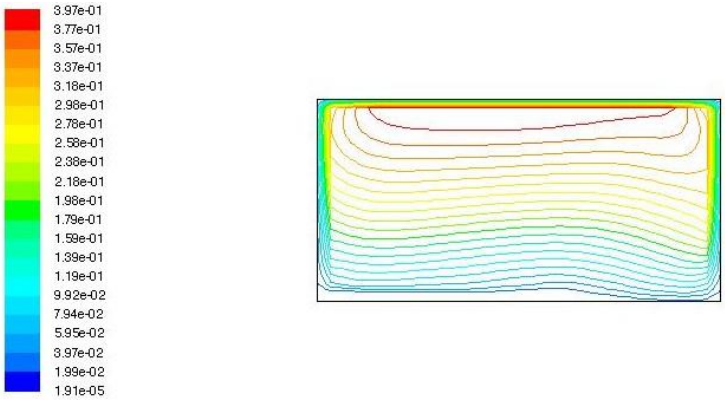

Figure 17: Contours of Turbulent Kinetic Energy for $Ra = 9.934 \times 10^{11}$

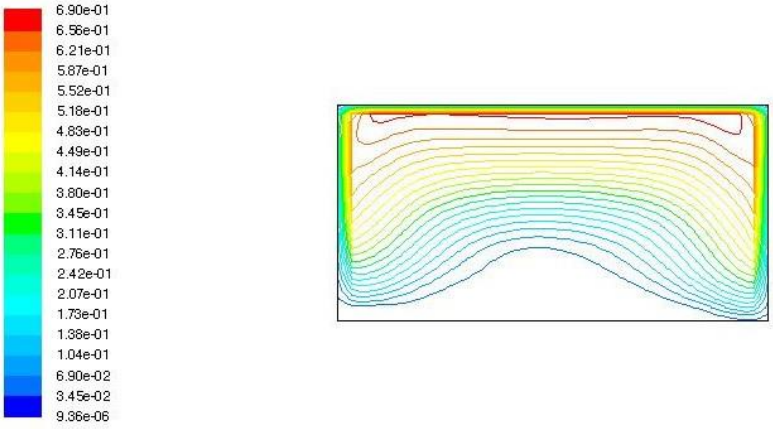

Figure 18: Contours of Turbulent Kinetic Energy for $Ra = 1.552 \times 10^{13}$

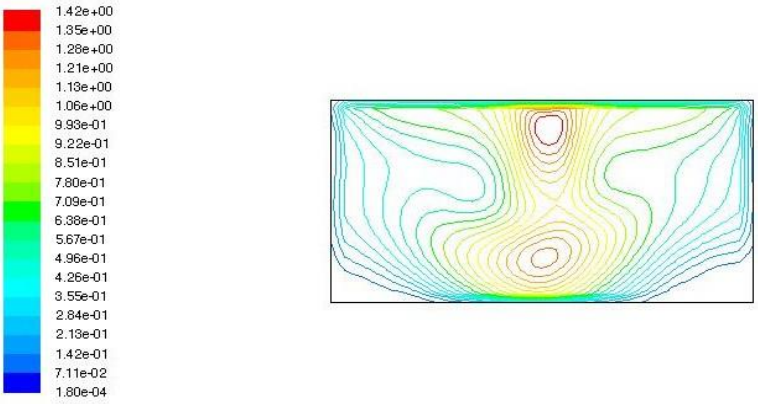

Figure 19: Contours of Turbulent Kinetic Energy for $Ra = 2.425 \times 10^{14}$

VII. Conclusion

The focus of this research was to use vorticity vector formulation to conduct a numerical simulation and investigation of natural turbulent flow inside a rectangular chamber filled with air. In order to accomplish this, we had established a number of specific objectives, all of which were met in the following ways:

In this work, we considered the partial differential forms of the Continuity Equation, the Navier-Stokes Equation, and the Energy Equation. These equations were statistically averaged and decomposed using the Reynolds Decomposition method. To complete the set of equations that defined turbulence, the resulting nonlinear equations comprising the Reynolds Stress equation were modeled by a k-ε turbulence model. Numeric data were set for k-ε turbulence model by application of vorticity stream function and vector potential formulation. The boussinesq estimation was used, which simplified the conservation equations. Three-point forward, central, and backward difference approximations discretized boundary-conditioned governing equations to numerically simulate the turbulent flow in the rectangular enclosure filled with air.

Streamlines, Velocity magnitudes, Isotherms and contours of kinetic energy were generated by FLU ENT 6.2.3 for Rayleigh numbers Ra = 1.552 × 1010, Ra = 9.934 × 1011, Ra = 1.552 × 1013 and

Ra = 2.425 × 1014 while keeping the aspect ratio of 2 constant. The results reveal that changing the Rayleigh number has an effect on fluid parameters including velocity and temperature. As a consequence of this, the magnitude of the velocity and the magnitude of the vortices both increase in tandem with an increase in the Rayleigh number. Maximum velocity was measured at 2.23 meters per second, and minimum velocity was measured at 0.308 meters per second.

For low Rayleigh numbers case, the temperature is higher than expected, and this is in relation to the way temperatures are distributed across the case. The flow becomes increasingly turbulent and chaotic as the Rayleigh number grows, which leads to the temperature being distributed toward the center of the enclosure. At the lowest Rayleigh number, the temperature reached a maximum of 290 degrees Kelvin, while at the highest Rayleigh number, the temperature reached a maximum of 279 degrees.

A rise in the Rayleigh number is responsible for the accompanying rise in kinetic energy. The results show that as the Rayleigh number increases, the kinetic energy of the fluid in the domain's turbulent regions also increases. In addition, the higher the value of the Rayleigh number, the greater the kinetic energy fluctuations, and thus the greater the fluid velocity of the liquid within the container. At high velocity regimes close to the heated wall, it

has also been discovered that the Rayleigh number has a considerable influence on the flow structure as well as the turbulent kinetic energy.

References

[1]. G. V. Kuznetsov and M. A. Sheremet, "Numerical simulation of turbulent natural convection in a rectangular enclosure having finite thickness walls.," International Journal of Heat and Mass Transfer, pp. 163-177, 2010.

[2]. P. Sompong and S. Witayangkurn, "Natural convention in a trapezoidal enclosure with wavy top surface.," Journal of Applied Mathematics, 2013.

[3]. R. Mayoyo, K. J. Sigey and M. J. Okwoyo, "An investigation of bouyancy driven natural convection in cylindrical enclosure.," 2015.

[4]. Z. Altaç and N. Ug˘urlubilek, Assessment of turbulence models in natural convection from two and three dimensional rectangular enclosures., International Journal of Thermal Sciences, 2016.

[5]. K. O. Awuor and M. G. Gicheru, "Numerical simulation of natural convection in rectangular enclosures.," 2017.

[6]. S. Karanja, J. Sigey, F. Gatheri and E. Kirima, "Turbulent natural convection in an enclosure at varying aspect ratio.," 2017.

[7]. H. Doukkali, S. Abide, M. Lhassane Lahlaouti and A. Khamlichi, "Large eddy simulation of turbulent natural convection in an inclined tall cavity.," Numerical heat transfer,Part A: Applications, pp. 1175-1189, 2018.

[8]. C. K. Mutua, "A numerical study of turbulent natural convection in a rectangular enclosure with localised heating and cooling.," 2019.

[9]. J. Liu, S. Hussain, W. Wang, G. Xie and B. Sundén, "Experimental and numerical investigations of heat transfer and fluid flow in a rectangular channel with perforated ribs.," International Communications in Heat and Mass Transfer., 2021.

[10]. K. Loksupapaiboon and C. Suvanjumrat, "Assessment of turbulence models for low turbulent natural convection heat transfer in rectangular enclosed cavity using openfoam.," In IOP conference series: Materials science and Engineering,, p. 012044, 2021.

[11]. R. Chaabane, L. Kolsi, A. Jemni, N. K. Alshammari and A. D'Orazio, "Numerical study of the Rayleigh-Benard convection in two dimensional cavities heated by elliptical heat sources using the lattice boltzmann method.," Physics of Fluids,, p. 33(12):123605, 2021.

[12]. D. Talukdar and M. Tsubokura, "Numerical study of natural convection from horizontal cylinder at eccentric position with change in aspect ratio of a cooled square enclosure.," Heat and Mass Transfer, pp. 1-23, 2021.

[13]. F. M. Mugambi, "Numerical simulation of turbulent natural convection in a rectangular enclosure with localised heating and cooling.," 2021.

[14]. P. S. Bernard and J. M. Wallace, Turbulent flow: Analysis, measurement and prediction., John wiley and sons, 2002.

[15]. H. Ozoe, K. Yamamoto, S. Churchill and H. Sayama, Three dimensional, numerical analysis of laminar natural convection in a confined fluid heated from below, 1976.

[16]. M. Kubíc˘ek, V. Hlavác˘ek and M. Holodniok, "Solution of non boundary value problems: The false transient method.," Chemical Engineering Science, pp. 31(8): 727-731, 1976.

[17]. M. DOG˘ AN and D. DOG˘ AN, "Experimental investigation of natural convection heat transfer from fin arrays for different tip-to-base fin spacing ratios," Isı Bilimi ve Teknig˘i Dergisi, pp. 27(1):147-157, 2017.